Biomaterials Science

ROYAL SOCIETY OF CHEMISTRY

PAPER

View Article Online
View Journal | View Issue

Cite this: *Biomater. Sci.*, 2021, **9**, 4717

^{18}F-Labeled magnetic nanovectors for bimodal cellular imaging†

Markus B. Schütz,[a] Alexander M. Renner,[a] Shaista Ilyas,[a] Khan Lê,[a] Mehrab Guliyev,[b] Philipp Krapf,[b] Bernd Neumaier[b] and Sanjay Mathur*[a]

Surface modification of nanocarriers enables selective attachment to specific molecular targets within a complex biological environment. Besides the enhanced uptake due to specific interactions, the surface ligands can be utilized for radiolabeling applications for bimodal imaging ensured by positron emission topography (PET) and magnetic resonance imaging (MRI) functions in one source. Herein, we describe the surface functionalization of magnetite (Fe_3O_4) with folic acid as a target vector. Additionally, the magnetic nanocarriers were conjugated with appropriate ligands for subsequent copper-catalyzed azide–alkyne cycloaddition or carbodiimide coupling reactions to successfully achieve radiolabeling with the PET-emitter ^{18}F. The phase composition (XRD) and size analysis (TEM) confirmed the formation of Fe_3O_4 nanoparticles (6.82 nm ± 0.52 nm). The quantification of various surface functionalities was performed by Fourier-transform infrared spectroscopy (FT-IR) and ultraviolet-visible microscopy (UV-Vis). An innovative magnetic-HPLC method was developed in this work for the determination of the radiochemical yield of the ^{18}F-labeled NPs. The as-prepared Fe_3O_4 particles demonstrated high radiochemical yields and showed high cellular uptake in a folate receptor overexpressing MCF-7 cell line, validating bimodal imaging chemical design and a magnetic HPLC system. This novel approach, combining folic acid-capped Fe_3O_4 nanocarriers as a targeting vector with ^{18}F labeling, is promising to apply this probe for bimodal PET/MR-studies.

Received 19th April 2021,
Accepted 9th May 2021

DOI: 10.1039/d1bm00616a

rsc.li/biomaterials-science

1. Introduction

Nanoparticles (NPs) of various compositions (*e.g.* metals, oxides, and lanthanide-doped) have gained significant attention in the field of biomedical imaging.[1–10] They are mainly used as contrast agents[11–16] following a significant function in numerous emerging applications such as photodynamic therapy, hyperthermia based cancer treatments or magnetic resonance imaging (MRI).[17] Magnetic NPs are favored as MRI contrast agents[18] due to their low cytotoxicity in the human body as validated by various clinical studies.[19–21] To this end, multimodal imaging and simultaneous therapy can provide complementary information for precise diagnosis and imaging-guided focused tumor therapy, which points out the need for dual-action probes with integrated imaging and therapeutic functions. Positron emission tomography[22–25] (PET) using positron emitters such as ^{11}C, ^{13}N, ^{18}F or ^{68}Ga is widely used in clinical practice for tumor detection or the elucidation of neurological disorders.[23,24,26–33] Fluor-18 is the most frequently applied radionuclide in diagnosis due to its favorable decay properties with a half-life of 109.8 min and low β^+-energy and should also be suitable for the labeling of NPs.[30,34–41]

The common strategies for producing radioactively labeled nanoparticles include either the labeling of the particle core or of the particle shell. For example, the core of iron oxide nanoparticles can be radioactively labeled by the nuclear reaction of ^{58}Fe(n,γ)^{59}Fe; however, due to the natural isotopic distribution of iron (91.72% ^{56}Fe, 2.2% ^{57}Fe and 0.28% ^{58}Fe), the labeling yield is very low, and the irradiation times are very long.[42] A promising alternative involves the co-precipitation of radioactive ^{59}Fe salts for synthesis, where the advantage lies in the high half-life time of ^{59}Fe ($t_{1/2}$ = 45d).[43] A more versatile method is the radioactive labeling of the organic periphery through surface-attached biomolecules, antibodies and other target ligands. Devaraj *et al.* reported on a synthetic route for the radioactive labeling of magnetic iron oxide nanoparticles with [^{18}F]Fluoride in which cross-linked dextran superparamagnetic iron oxide nanoparticles were modified with an ^{18}F-PEG$_3$ radiotracer.[30] However, the combination of magnetic iron oxide nanoparticles and the [^{18}F]Fluoride radiotracer

[a]*Institute of Inorganic Chemistry, University of Cologne, D-50939 Cologne, Germany. E-mail: sanjay.mathur@uni-koeln.de; Tel: +49 221 470 5627*
[b]*Institute of Neuroscience and Medicine-Nuclear Chemistry (INM-5), Forschungszentrum Jülich, D-52428 Jülich, Germany*

†Electronic supplementary information (ESI) available. See DOI: 10.1039/d1bm00616a

remains elusive due to the orthogonality of functional characteristics and prerequisites of the biomedical imaging protocols.

Folate receptors (glycophosphatidylinositol, FRs) are recognized as a useful therapeutic site due to their overexpression in many tumor sites including those in lung, colon, breast and ovarian cancers.[44] This membrane protein binds to folic acid with high affinity and facilitates its intracellular transport *via* the endocytic process. Consequently, folic acid has been considered as a potential target ligand for the directed delivery of their payloads to cancer cells.[44,45] We report here on alkyne-functionalized magnetic nanoparticles for subsequent "click" conjugation[46] for radiolabeling exhibiting promising labeling yields and site-specific cellular uptake. The carbodiimide coupling reaction was performed on the surface of magnetic carriers to attach folic acid for directing the dual-action labels to the site of interest. In addition, we also report for the first time an innovative purification strategy that efficiently separates nanoparticles from starting materials and unbound radioactive molecules to visualize radioactively labeled particles. The dual-mode labels can be used for magnetic resonance imaging (MRI) and positron emission tomography (PET) studies to demonstrate their potential in selective targeting and bimodal imaging.

2. Results and discussion

Magnetite (Fe_3O_4) nanoparticles with different surface functionalities were synthesized by the hydrothermal decomposition of an iron(III) salt in the presence of sodium ascorbate as the surfactant and reducing agent, 4-(chloroacetyl)catechol (AACl) and dopamine (Fig. 1, step 1). The *in situ* reduction of the Fe(III) species (to Fe(II)) was controlled by adding a stoichiometric amount of the reducing agent. The catechol function of the ligand molecules is essential for the functionalization since it has a strong binding affinity to iron oxides that enabled a stable surface attachment.[47] Folic acid was coupled to dopamine amino groups exploiting carbodiimide chemistry (Fig. 1, step 3) as a targeting molecule for cancer cells with overexpressed folate receptors. The chloride of the AACl was substituted by an azide group (Fig. 1, step 2) for the subsequent azide–alkyne cycloaddition reaction. Two different pathways were explored for the radiolabelling. In the first approach, the tosylate (OTs) leaving group needed for subsequent labeling with ^{18}F (Fig. 1, step 5) was conjugated by coupling pent-4-ynyl tosylate to the introduced azide moiety by a copper-catalyzed azide–alkyne cycloaddition (Fig. 1, steps 4 + 5) and the radiolabelling was conducted afterwards. For the other pathway, the radiolabelling building block (^{18}F-pent-4-ynyl) was pre-synthesized separately and then coupled to the azide bound to the nanoparticles (Fig. 1, step 2) using the same copper-catalyzed cycloaddition as before.

The as-obtained nanoparticles displayed a spherical shape that was verified by transmission electron microscopy showing an average size of 6.82 nm ± 0.52 nm. The observed agglomeration in the coated iron oxide nanoparticles is possibly due to their ultra-small size and the inherent magnetic properties of Fe_3O_4 (Fig. 2A). The powder X-ray diffraction data confirmed the formation of phase pure Fe_3O_4 particles (Fig. 2B). The NPs showed enhanced colloidal stability after surface conjugation with dopamine and 4-(chloroacetyl) catechol ligands displaying an average hydrodynamic radius of 171.10 nm ± 2.51 nm as determined by DLS measurements. The infrared spectra displayed the (Fig. 2C) vibrational bands corresponding to both surface ligands. The Fe_3O_4 NPs coated with only dopamine possessed a ζ-potential in a positive range (25.90 mV ± 0.25 mV) due to the presence of protonated amino groups on the surface, whereas after modification with AACl, the surface ζ-potential shifted to negative values (−35.2 mV ± 1.01 mV). Consequently, the surface modification of NPs with both dopamine and AACl ligands led to a less negative ζ-potential of −21.35 mV ± 0.29 mV (Fig. 2E).

The terminal chloride groups of the AAC molecules attached on the surface were replaced by azide groups in a S_N2 nucleophilic substitution reaction. The substitution reaction was confirmed by the observation of the characteristic azide vibration band at a wavenumber of 2100 cm^{-1} (Fig. 2C). Additionally, the ζ-potential change from −21.35 mV ± 0.29 mV to −12.20 mV ± 0.53 mV also suggested a change in the surface chemistry upon individual functionalization steps (Fig. 2E). The presence of surface-terminating azide groups was necessary to conjugate alkynated-^{18}F for the radiolabeling study following the click-chemistry protocol. Furthermore, the amino functionality was used to perform a carbodiimide coupling reaction for the attachment of folic acid which is a UV active targeting ligand. In the consequent steps, the NPs were tested for different concentrations of folic acid (0.25 mg mL^{-1}, 0.5 mg mL^{-1}, 2.5 mg mL^{-1}, 5 mg mL^{-1}) by performing conjugation reactions under similar reaction conditions. Different amounts of folic acid units immobilized on the surface of the nanoparticles were verified by absorption spectra and through the changes in the UV/Vis maxima as a function of the initial quantity of the ligand, as is evident in Fig. 2D. The intensity of λ_{max} in the wavelength range of 272 nm to 282 nm showed a significant decrease depending upon the additional folic acid in the reaction. The ζ-potential changed from −12.20 mV ± 0.53 mV to 32.62 mV ± 0.38 mV indicating a significant alteration of the chemical topography of the particles. The folic acid molecule has several $-NH_2$ groups that can be protonated in aqueous solution that accounts for the significant change in the ζ-potential.

In order to perform radiolabeling experiments, azide groups of the modified Fe_3O_4 particles were used following two different methods. In the first approach, pent-4-ynyl tosylate (tosylate leaving group)[48] was coupled to the surface of the nanoparticles using the "click" reaction followed by direct labeling with the radioactive ^{18}F label. The outcome of the reaction was confirmed by ζ-potential and IR measurements. In the IR spectra, the observable decrease of the azide signal at a wavenumber of 2100 cm^{-1} was visible, indicating the coupling of the azide moiety with alkyne groups of pent-4-ynyl tosy-

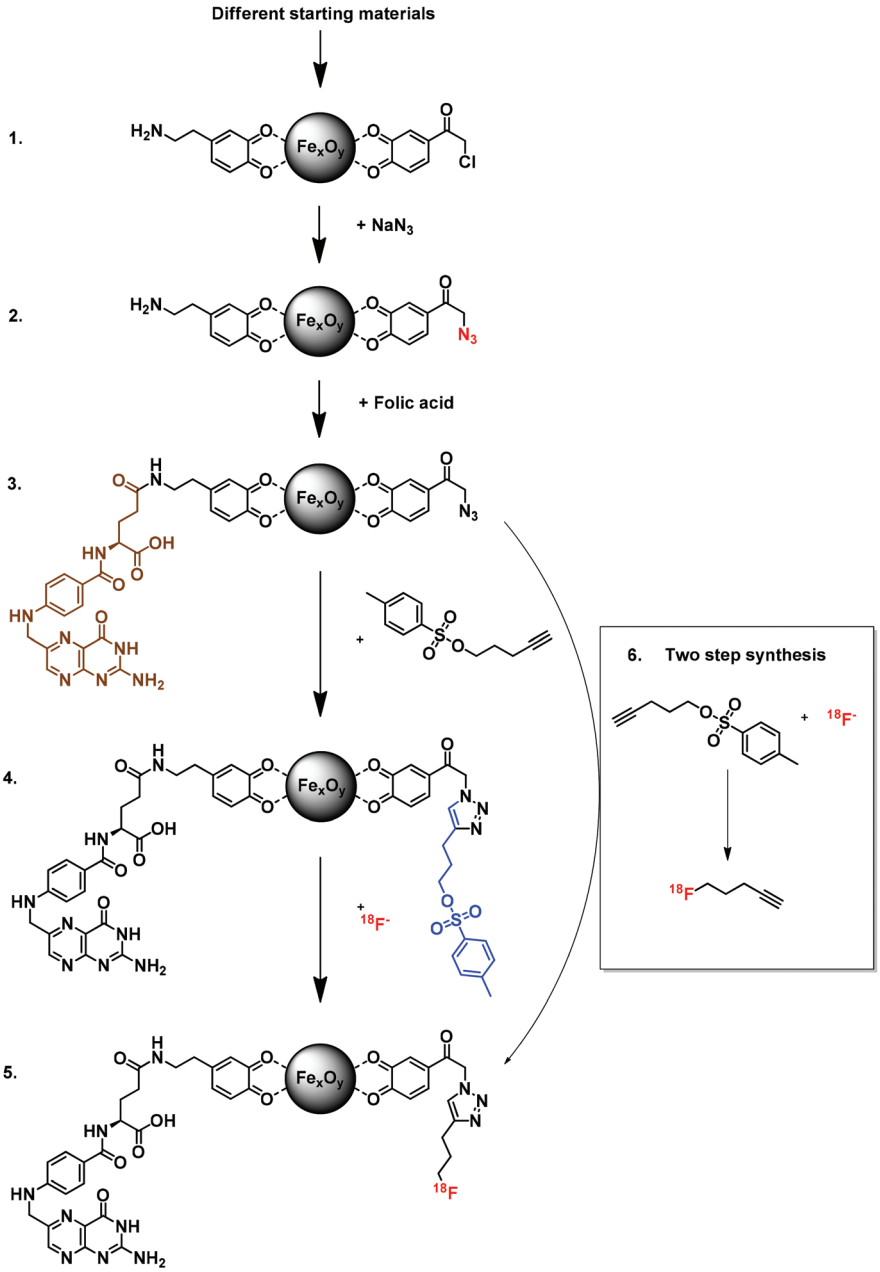

Fig. 1 Reaction scheme for the synthesis and functionalization of Fe_3O_4 nanoparticles following radioactive labeling with ^{18}F by two different reaction pathways. Pathway "1–5" is a direct labeling approach where the tosylate leaving group is attached to the NPs by the azide–alkyne coupling before ^{18}F labeling. Pathway "1–3. +6" includes the external ^{18}F labeling and subsequent coupling with the labeled building block.

late. The specific bands for the triazole group with a wavenumber between 1290 and 825 cm^{-1} could not be clearly detected due to an overlap with other bands in the spectra. The ζ-potential shifted from 32.62 mV ± 0.38 mV to 20.76 mV ± 0.57 mV. The magnitude of the ζ-potential indicated the potential high stability of colloidal nanoconjugates. Additionally, the colloidal stability was characterised and was in a range of 60 min to 420 min. The FA-AAN_3@Fe_3O_4 and AACl@Fe_3O_4 particles showed the highest stability in water.

In the second approach, the magnetic particles were separated from the reaction chamber after the conjugation of ^{18}F labeled pent-4-ynyl tosylate (OTs) followed by the click reaction. The success of the radiolabeling reaction between azide modified particles and alkynated radioactive ligands was controlled using radio-HPLC. The results confirmed that after the purification step by distillation only the radioactive product was present in the reaction chamber that validated the efficacy of the magnetic separation approach.

In comparison with radioactive labeled proteins or small molecules, nanoparticles have solid surfaces and they tend to agglomerate in different solvents due to interparticle interactions. The appropriate use of a conventional HPLC system

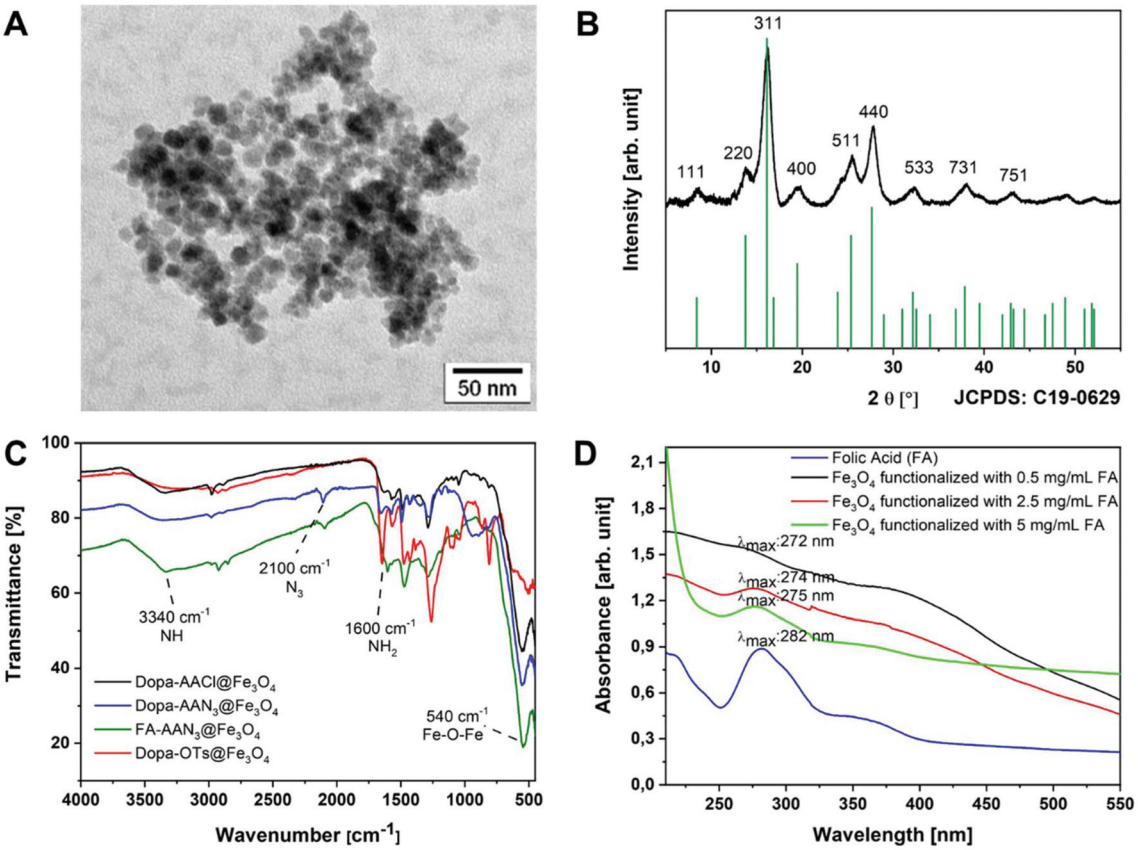

E

Sample	Zeta Value [mV]
$Dopa@Fe_3O_4$	+25.90 ± 0.25
$AACl@+Fe_3O_4$	-35.2 ± 1.01
$Dopa\text{-}AACl@Fe_3O_4$	-21.35 ± 0.29
$Dopa\text{-}AAN_3@Fe_3O_4$	-12.20 ± 0.53
$FA\text{-}AAN_3@Fe_3O_4$	+32.62 ± 0.38
$FA\text{-}OTs@Fe_3O_4$	+20.76 ± 0.57

Fig. 2 (A) TEM image of the as-synthesized iron oxide NPs with an average size of 6.82 nm. (B) XRD pattern of the as-synthesized Fe_3O_4 NPs. (C) Infrared spectrum of the NPs before and after the functionalization with Dopa and OTs. (D) UV-Vis spectra for surface group analysis before and after the functionalization of magnetite NPs with different concentrations of folic acid molecules. (E) Table containing the ζ-potential values of functionalized NPs. The pH values of particle dispersions were in the range of 5.5 to 6.5.

with a suitable separation column is not effective because a controlled passage through the column cannot be guaranteed for particle agglomerates that poses a high risk of blocking the pores of the whole system. Therefore, in this work an innovative set-up was developed for cleaning magnetic nanoparticles, which could be successfully used for radioactive labeled particles as well. For this purpose, instead of the column, a permanent magnet was added to the HPLC system, while the other parts remained the same as shown in Fig. 3. A tube wrapped around the magnet leads to the accumulation of the magnetic particles next to the magnet. All nonmagnetic starting materials or side products were washed out continuously. After removing the magnet, the collected magnetic particles were washed out from the tube and detected with a scintillation detector. This cleaning setup was evaluated with two other HPLC systems with different magnetic nanoparticles that confirmed its versatility for the separation of magnetic NPs.

To evaluate the radioactive yield of the folic acid and ^{18}F labeled nanoparticles, different reaction parameters were developed. It was possible to increase the radiochemical yield up to 15% with acetonitrile as the solvent during the radio-

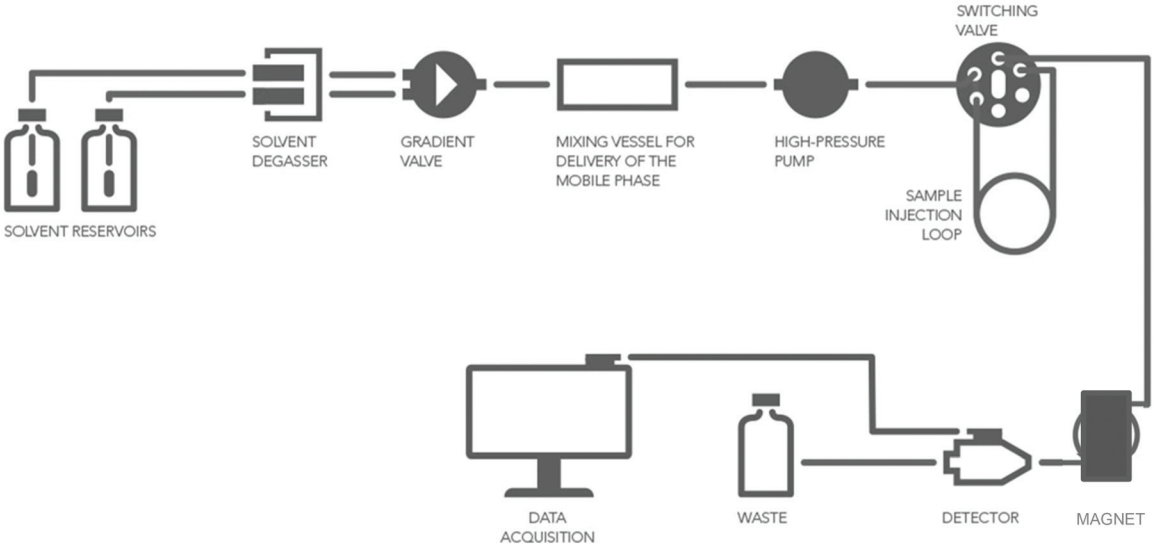

Fig. 3 Schematic construction of the HPLC system with a new component for the separation of magnetic nanoparticles.

active labeling. A number of other common solvents that are typically used for nanoparticle dispersions were also analyzed to define the most suitable solvent system. The utilization of MeOH (0.3%), DMF (2.4%), DMA (1.7%), diethylether (0.13%), DMSO (0.43%), *tert*-butyl alcohol (0.7%), EtOH (0.13%), water (0%), ACN/water (7.47%) and ACN/EtOH (3.47%) led to a lower radiochemical yield (Fig. 4).

It is necessary to select an appropriate number of input parameters such as reaction temperature and time to evaluate the effectiveness of the labeling yield. The collective assessment of these parameters showed (Fig. 5) an increase in the labeling efficiency from 0 min to 30 min at a temperature of 80 °C. An increase in the reaction time up to 60 min was found to provide 1.09% higher yield. The increase in the temperature from 80 °C to 110 °C did not affect the yield, which shows that surface conjugation is quantitatively achieved already at 80 °C. In conclusion the radioactive labeling gave the best results in acetonitrile at 80 °C with a reaction time of 30 min as shown in Fig. 5.

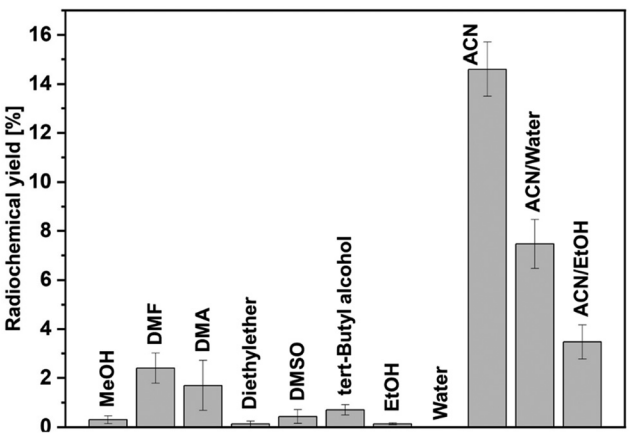

Fig. 4 Graphical evaluation of the radiochemical yield of ^{18}F labeled magnetite NPs in various solvents.

After establishing the optimal reaction conditions, the nanoparticles with different concentrations of folic acid surface-ligands were labeled in a one-step approach. The particles with the lowest amount of folic acid (0.50 mg mL^{-1}) showed the weakest radioactive yield (2.5%) after a reaction at 80 °C for 30 min. The results showed that the radioactive yield increases in relation to the amount of folic acid attached on the surface of the nanoparticles (2.50 mg mL^{-1}: 6% RCY, 5.00 mg mL^{-1}: 13% RCY). Therefore, the steric hindrance of folic acid is unlikely to have a significant impact in the examined system, as a reduced amount of folic acid did not increase the radioactive yield.

The one-step labeling offers several benefits in comparison with the multistep labeling approach. Firstly, the RCY is higher (15% compared to 7%) and the overall reaction time is shorter enabling more efficient use of ^{18}F which is a crucial parameter due to the short half-life of the radionuclide. Secondly, the two-step reaction requires an additional cleaning step after the synthesis of the radiolabeled ligand, resulting in higher losses of particles and the decay of ^{18}F.

The versatility of the surface conjugation and magnetic separation approaches developed in this work was demonstrated for another nanoparticle type by using the same surface chemistry and labeling protocols. The γ-Fe_2O_3 nanoparticles with pronounced magnetic properties and an average size of 250 nm ± 2 nm were synthesized by solution processing to obtain a crystalline material that was confirmed by powder XRD data, which showed the presence of a minor phase that could not be unambiguously detected (Fig. 6A & B). The particles were tested for a click reaction between 4-(azidoacetyl) catechol and pent-4-ynyl tosylate. After the functionalization, IR-measurements showed the introduced catechol ligand with a stretching frequency at a wavenumber of 2100 cm^{-1} indicat-

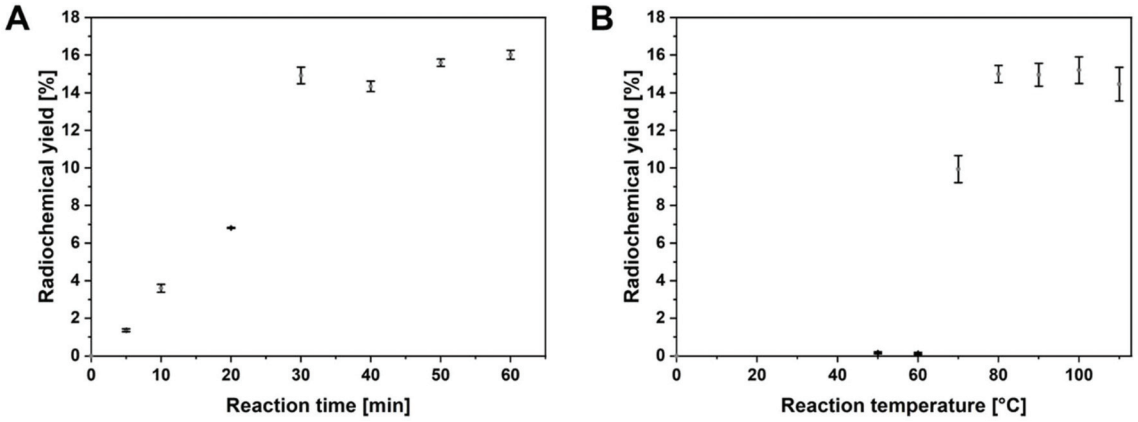

Fig. 5 Optimization of the (A) reaction time and (B) reaction temperature for the radioactive labeling of magnetite nanoparticles with ^{18}F in acetonitrile.

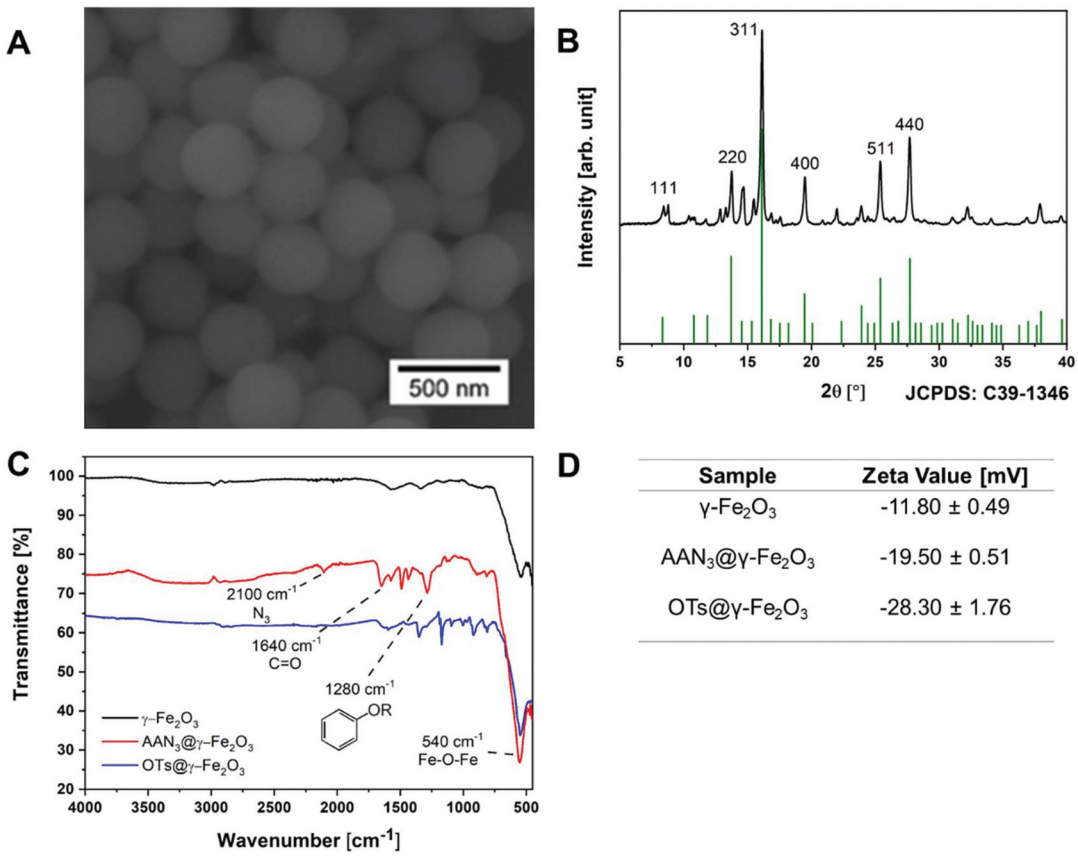

Sample	Zeta Value [mV]
γ-Fe_2O_3	-11.80 ± 0.49
AAN_3@γ-Fe_2O_3	-19.50 ± 0.51
OTs@γ-Fe_2O_3	-28.30 ± 1.76

Fig. 6 (A) SEM image of the as-synthesized γ-Fe_2O_3 NPs. (B) XRD pattern of the as-synthesized Fe_2O_3 NPs. (C) Infrared spectrum of the NPs before and after the functionalization with AAN_3 and OTs. (D) Table containing the ζ-potentials of functionalized NPs.

ing the presence of the azide function (Fig. 6C). After the click reaction this vibration band disappeared due to the transformation of the azide moiety into a triazole group. The signals for the catechol ligand in an area between 1500 and 1750 cm^{-1} appeared as somewhat blurred bands. The ζ-potential of the nanoparticles shifted from −11.80 mV ± 0.49 mV to −19.50 mV ± 0.51 mV after functionalization with 4-(azidoacetyl)catechol that changed to −28.30 mV ± 1.76 mV after the completion of the click reaction (Fig. 6D).

After radiolabeling with ^{18}F under conditions optimized for magnetite particles, the NPs demonstrated a radiochemical yield of 37.79% ± 2.78%. The higher yield in comparison with that with the folic acid-labeled particles is possibly due to the larger size of the particles and the additional higher amount

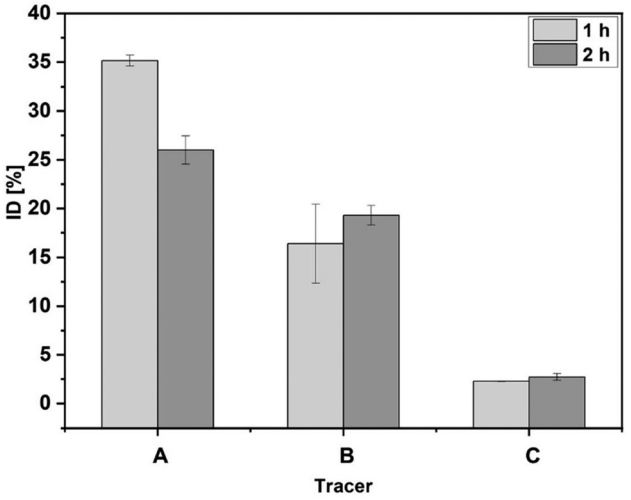

Fig. 7 Cellular uptake of different radiolabeled materials by MCF-7 cells after 1 and 2 h. The cell concentration was 100 cells per µL. Tracer: (A) [^{18}F]Folic Acid@Fe_3O_4 NPs; (B) [^{18}F]NH_2@Fe_3O_4 NPs; (C) [^{18}F]FET.

of azide groups on the surface. In comparison, there are no additional extra dopamine groups on the surface which leads to more OTs leaving groups which can react with the free ^{18}F. The attractive labelling yield for these particles shows the practicability of this method that will be useful for nanomedicine and can be adapted for the functionalization and radiolabelling of several other magnetic particles with different shapes and surface properties.

The cellular uptake of radiolabeled nanoparticles was carried out in triplicate (n = 3) with MCF-7 cancer cells (Fig. 7). The ^{18}F-labeled and folic acid modified Fe_3O_4 nanoparticles showed a 35.15% ± 0.56% efficiency after one hour and a 26.00% ± 1.46% efficiency after two hours of application. For the control sample ^{18}F-labelled Fe_3O_4 nanoparticles without folic acid functionalization were used and a lower uptake (2 h: 19.3% ± 0.99%, 1 h: 16.4% ± 4.03%) was observed. The higher cellular uptake for the folic acid functionalized nanoparticles is possibly due to the overexpression of folate receptors in the MCF-7 cells and is proof for the successful functionalization.[49] These observations suggest that the cellular uptake of nanoparticles followed receptor mediated endocytosis.

In comparison with the standard tracer [^{18}F]FET which is used especially for brain tumors, the nanoparticle described here showed a higher cellular uptake than the results known for the standard tracer (2 h: 2.73% ± 0.35%, 1 h: 2.28% ± 0.03%) probes, which are evidently much weaker. This demonstrates the potential of radioactive-labelled nanoparticles for cellular imaging and can be tested for the *in vivo* cellular imaging of cancer cells.

3. Conclusions

Hydrothermally synthesized magnetic nanoparticles (Fe_3O_4 and γ-Fe_2O_3) were successfully labelled with ^{18}F-radioactive nuclides and conjugated with folic acid as target ligands following click chemistry protocols. Precisely, a chemical conjugation approach provided a facile pathway to immobilize tosylate groups on the outer surface of carrier nanoparticles for grafting radiolabeled ligands. The ^{18}F-labelled particles were separated and purified in an improved HPLC system developed in this work. Comprehensive characterization of surface-attached functional groups and solution behavior by IR, ζ-potential, and DLS analyses confirmed the presence of amino- and azido-units that could be selectively activated by carbodiimide coupling and cycloaddition reactions to obtain novel dual-action magnetic probes suited for simultaneous MRI and PET imaging. The attachment of different amounts of folic acid units on the surface of nanoparticles by carbodiimide coupling showed that steric hinderance does not play any predominant role in the radiolabeling of nanoparticles and the complementarity of the reaction partners is decisive for obtaining dual-action radioactive magnetic carriers. The challenge of separating the bimodal PET-MRI tracer from the unlabeled nanoparticles and excess ligands was addressed by developing a novel, efficient and economical modification in the HPLC set-up that demonstrated the separation efficiency and detection of purified radiolabeled nanoparticles from the starting materials. This component can be useful for the differentiation of nanoparticles suspended in various organic solvents for radioactive labeling protocols. The study of radiolabeling efficiency in various solvent systems showed acetonitrile to be most promising with the highest radiolabeling yield (>15%) at 80 °C after 30 min. Additionally, the radioactive and folic acid labeled nanoparticles showed higher receptor-mediated endocytosis of particles in comparison with the particles without folic acid used as the reference. Finally, it was demonstrated that co-conjugated nanoparticles bearing target ligands and a PET source have extraordinary potential for cellular imaging as compared to standard radiotracers. The results reported here demonstrate the translational potential of magnetic nanocarriers as bimodal tracer systems that can be further improved by attachment of multiple radiotracers.

4. Experimental section

Instrumentation

Nuclear magnetic resonance (NMR) spectroscopy. ^{1}H- and ^{13}C-NMR spectra were recorded at 300 MHz and 75 MHz, respectively. The measurements were performed on a Bruker AV 300 MHz (Billerica, Massachusetts, USA). The chemical shifts δ are reported in ppm downfield of the internal standard of TMS [δ (^{1}H-NMR) = 0.00 ppm, δ (^{13}C-NMR) = 0.00 ppm]. $CDCl_3$ [δ (1H-NMR) = 7.24 ppm, δ (^{13}C-NMR) = 77.2 ppm] and DMSO-d_6 [δ (^{1}H-NMR) = 2.50 ppm, δ (^{13}C-NMR) = 39.5 ppm] were used as solvents. The coupling constant J is indicated in Hz. The fine structure is designated using the following abbreviations: s (singlet), d (doublet), t (triplet), q (quartet), quin (quintet), sxt (sextet), sep (septet), br (broad) and m (multiplet).

X-ray diffraction (XRD). XRD measurements were performed on a STOE-STADI MP diffractometer (STOE & Cie GmbH, Darmstadt, Germany) with a Mo-source (Kα = 0.71073 Å). The obtained signals were then compared to JCPDS-data. WinXPOW (STOE & Cie GmbH, Darmstadt, Germany) software was used to evaluate the diffractograms.

ζ-Potential and dynamic light scattering (DLS). ζ-Potential and DLS measurements were performed on a Zetasizer Nano ZS (Malvern Instruments, Malvern, UK; λ = 633 nm). Each sample was highly diluted and dispersed in water. Samples were measured in triplicate at 25 °C.

Transmission electron microscopy (TEM). TEM images were taken with a LEO 912 (Zeiss, Oberkochen, Germany). A highly diluted dispersion of each sample in ethanol was prepared. Images were taken after evaporation of the solvent.

UV/Vis-spectroscopy. The UV/Vis-experiments were performed on a Lambda 950 (PerkinElmer, MA, USA) at room temperature. All samples were dissolved or dispersed in water.

Fourier-transform infrared spectroscopy (FTIR). The IR spectra were recorded using an FT-IR spectrometer Spotlight 400 FTIR Imaging System from the company Perkin Elmer (MA, USA). All measurements were performed under air conditions at room temperature in a range from 400 to 4000 cm^{-1}. For the graphics the program Origin was used.

Scattering electron microscopy (SEM). All SEM images were recorded using Nova NanoSEM from the company FEI. For sample preparation the particles were dissolved in ethanol and dried on silicon wafer.

High performance liquid chromatography (HPLC) analysis. HPLC analysis was carried out using two different systems:

(1) Dionex Ultimate 3000, Thermo Fisher Scientific with an integrated UV-detector in combination with a radio detector HERM LB 500 (high energy radio monitor) (Berthold Technologies, Bad Wildbad, Germany).

(2) Knauer pump, a Knauer K-2500 UV/VIS detector (Knauer, Berlin, Germany) a manual Rheodyne injector (1 ml loop) and a NaI(Tl) well-type scintillation detector (EG&G Ortec; modul 276 Photomultiplier Base) with an ACE Mate Amplifier and BIAS supply (all from Ortec Ametek, Meerbusch, Germany). Data acquisition and interpretation were performed using Gina software (Raytest).

Chemicals. All reagents and solvents used were obtained from commercial sources (Sigma Aldrich, Alfa Aesar, Fisher Scientific, Carbolution, Linde, Tokyo Chemical Industry Co. Ltd and Acros Organics). The purity of the reagents used was at least 95% and these were used without further purification. All moisture and/or oxygen sensitive reactions were carried out under a nitrogen atmosphere. (4-(Chloroacetyl)catechol – TCI, NaN_3 – Sigma Aldrich, $FeCl_3{\cdot}6\ H_2O$ – Sigma Aldrich, $NaHCO_3$ – Alfa Aesar, dopamine – Sigma Aldrich, dicyclohexylcarbodiimide – Sigma Aldrich, *N*-hydroxysuccinimide – Alfa Aesar, pent-4-ynyl tosylate – Sigma Aldrich, $CuSO_4{\cdot}5\ H_2O$ – Sigma Aldrich).

Methods

Synthesis of fluor-18. [^{18}F]Fluorid was produced by the $^{18}O(p,n)^{18}F$ reaction by bombardment of enriched [^{18}O]H_2O with 16.5 MeV protons using a BC1710 cyclotron (The Japan Steel Works Ltd, Shinagawa, Japan) at the INM-5 (Forschungszentrum, Jülich).

Synthesis of 4-(azidoacetyl)catechol. 500 mg of 4-(chloroacetyl)catechol (2.7 mmol, 1 eq.) was dissolved in 4 mL of anhydrous DMF. To this solution, 210 mg of NaN_3 (3.23 mmol, 1.2 eq.) was added and the solution was stirred for 2 h at ambient temperature. Then 10 mL of EtOAc was added and the mixture was washed with water three times. The collected organic layer was dried with anhydrous $MgSO_4$. The crude product was washed with a hexane/ether = 5/1 solution and evaporated under vacuum. The white solid was obtained in a yield of 320 mg (62%). The obtained catechol derivative was analyzed by ^{1}H-NMR and IR spectroscopy.

Synthesis of dopamine + 4-(chloroacetyl)catechol (AACl) @Fe_3O_4 nanoparticles. 0.57 g of $FeCl_3{\cdot}6\ H_2O$ was dissolved in 10 mL of H_2O and stirred for 10 min at ambient temperature. 1.35 g of $NaHCO_3$ were dissolved in 10 mL of H_2O and added slowly to the iron solution and the solution was stirred for 30 min at ambient temperature. Finally, 0.18 g of AACl and 0.19 g of dopamine were dissolved in 10 mL of H_2O and added. The solution was stirred for an additional 30 min at room temperature. Afterwards the solution was transferred into a Teflon tube and autoclaved at 200 °C for 6 h. The particles were washed several times by centrifugation at 11 000 rpm for 30 min and redispersed in H_2O/EtOH. The Fe_3O_4 nanospheres were analysed by XRD, IR, DLS/Zeta measurements and images were recorded using SEM/TEM. The particles were used for surface modification with NaN_3, folic acid and pent-4-ynyl tosylate and subsequently radiolabelled.

Synthesis of PEG-stabilized γ-Fe_2O_3 nanospheres. 0.81 g of $FeCl_3{\cdot}6\ H_2O$ was mixed with 2.64 g of NaAc·3 H_2O, 1.154 g of SDS and 0.4 g of PEG 6000 in 24 mL of ethyleneglycol. The mixture was transferred into a Teflon tube and autoclaved at 180 °C for 6 h. The particles were washed seven times by centrifugation at 11 000 rpm for 30 min and redispersed in H_2O/EtOH. The Fe_3O_4 nanospheres were analysed by XRD, IR, DLS/Zeta measurements and images were recorded using SEM/TEM. The particles were used for surface modification with 4-(azidoacetyl)catechol and subsequent radiolabeling.

Synthesis of 4-(azidoacetyl)catechol@γ-Fe_2O_3 nanospheres. 10 mg of Fe_3O_4 nanospheres were dispersed in 5 mL of heptane and 100 mg of 4-(azidoacetyl)catechol were added. The mixture was kept in an ultrasonic bath for 30 min and then centrifuged 5 times at 11.000 rpm for 30 min, redispersing the particles in H_2O/EtOH after each centrifugation. The surface modified particles were analyzed by XRD, DLS/Zeta and IR spectroscopy. They were used for radiolabeling.

Synthesis of dopamine + 4-(azidoacetyl)catechol@Fe_3O_4 nanoparticles. 10 mg of dopamine + AACl@Fe_3O_4 nanoparticles were dispersed in 5 ml of anhydrous DMF and 50 mg of NaN_3 were added. The mixture was stirred overnight at room temperature and then centrifuged 5 times at 11 000 rpm for 30 min, redispersing the particles in H_2O/EtOH after each centrifugation. The surface modified particles were analyzed by XRD, DLS/Zeta and IR spectroscopy. They were used for

surface modification with folic acid and pent-4-ynyl tosylate and subsequently radiolabelled.

Synthesis of folic acid + 4-(azidoacetyl)catechol@Fe_3O_4 nanoparticles.[50] Folic acid was attached to the particle surface by carbodiimide coupling. Therefore, folic acid (5–50 mg) was mixed with 24 mg of dicyclohexylcarbodiimide (DCC) and dissolved in 5 ml of anhydrous DMSO. The mixture was stirred under a N_2 atmosphere for 3 h at room temperature. Afterwards 13 mg of *N*-hydroxysuccinimide (NHS) were added and the mixture was stirred for 24 h at room temperature. 15 mg of dry dopamine + 4-(azidoacetyl)catechol@Fe_3O_4 nanoparticles were dispersed in 5 ml of anhydrous DMSO and added to the activated folic acid mixture and stirred at room temperature for another 24 h. The particles were centrifuged 5 times at 11 000 rpm for 30 min and redispersed in H_2O/EtOH after each step. In the next steps they were used for surface modification with pent-4-ynyl tosylate and subsequently radiolabelled. The particles were analyzed by XRD, DLS/Zeta, IR spectroscopy and UV/vis measurements.

Synthesis of pent-4-ynyl tosylate.[51] To a cooled down solution in an ice bath of TsCl (3.84 g, 20.1 mmol, 1.00 eq.) in dry pyridine (17 ml), 4-pentyn-1-ol (1.70 g, 20.1 mmol, 1.00 eq.) was added under a nitrogen-atmosphere, stirred for 2 h at 0 °C and another 30 min at room temperature. Subsequently 30 ml of dest. H_2O were added to the solution and extracted three times with diethyl ether (30 ml each time). The combined organic layers were dried over $MgSO_4$ and the solvent was removed under reduced pressure. In a final step, the raw product was purified by column chromatography with a c-Hex/EtOAc-mixture (3 : 1) to obtain the product as a pale-yellow oil with a yield of 2.24 g (9.40 mmol, 47%). The product was analyzed by NMR spectroscopy and was used for radiolabeling.

Synthesis of tosylate@γ-Fe_2O_3 nanospheres. The surface modification with pent-4-ynyl tosylate was carried out using copper-catalyzed Huisgen cycloaddition. Therefore, stock solutions of $CuSO_4$, L-histidine and NaAs were prepared to reduce the weighting error. 25 mg of $CuSO_4{\cdot}5\ H_2O$ (0.1 mmol), 39 mg of L-histidine (0.25 mmol) and 98 mg of NaAs (0.49 mmol) were dissolved in 500 μL of H_2O each. 10 mg of pent-4-ynyl tosylate was mixed in this order with 50 μl of $CuSO_4{\cdot}5\ H_2O$ solution, 5 μL of L-histidine solution and 50 μL of NaAs solution. 10 mg of 4-(azidoacetyl)catechol@γ-Fe_2O_3 nanospheres were dispersed in dest. H_2O and added. The mixture was stirred for 18 h at ambient temperature. The particles were centrifuged 5 times at 11 000 rpm for 30 min and redispersed in H_2O/EtOH after each step. In the next step they were used for radiolabeling with $^{18}F^-$. The particles were analyzed by XRD, DLS/Zeta and IR spectroscopy.

Synthesis of folic acid + tosylate@Fe_3O_4 nanoparticles. Similar to the synthesis of the tosylate@γ-Fe_2O_3 nanospheres, the pent-4-ynyl was attached to the folic acid + 4-(azidoacetyl) catechol@Fe_3O_4 nanoparticles. 10 mg of pent-4-ynyl tosylate was mixed in this order with 50 μl of $CuSO_4{\cdot}5\ H_2O$ solution, 50 μL of L-histidine solution and 50 μL of NaAs solution. Folic acid + 4-(azidoacetyl)catechol@Fe_3O_4 nanoparticles were dispersed in dest. H_2O and added. The mixture was stirred for 18 h at ambient temperature. The particles were centrifuged 5 times at 11.000 rpm for 30 min and redispersed in H_2O/EtOH after each step. In the next step they were used for radiolabeling with $^{18}F^-$. The particles were analyzed by XRD, DLS/Zeta and IR spectroscopy.

Synthesis of tosylate + dopamine@Fe_3O_4 nanoparticles. Similar to the synthesis of the tosylate@γ-Fe_2O_3 nanospheres and folic acid + tosylate@Fe_3O_4 nanoparticles, pent-4-ynyl tosylate was attached to the dopamine + 4-(azidoacetyl) catechol@Fe_3O_4 nanoparticles. 10 mg of pent-4-ynyl was mixed in this order with 50 μl of $CuSO_4{\cdot}5\ H_2O$ solution, 50 μL of L-histidine solution and 50 μL of NaAs solution. Dopamine + 4-(azidoacetyl)catechol@Fe_3O_4 nanoparticles were dispersed in dest. H_2O and added. The mixture was stirred for 18 h at ambient temperature. The particles were centrifuged 5 times at 11.000 rpm for 30 min and redispersed in H_2O/EtOH after each step. In the next step they were used for radiolabeling with $^{18}F^-$. The particles were analyzed by XRD, DLS/Zeta and IR spectroscopy.

Radiosynthesis

Synthesis of 5-[^{18}F]Fluoro-1-pent-4-ynyl. Aqueous [^{18}F] Fluorid was trapped on a SepPAK Light Water Accell™ Plus QMA cartridge (Waters GmbH, Eschborn, Germany), washed with methanol (1 ml), and eluted with tetraethylammonium bicarbonate solution (5 mg in 500 μl MeOH). Methanol was evaporated under an argon stream at 40 °C and 500 mbar within 2–4 min. After cooling to room temperature, the residue was mixed with pent-4-ynyl tosylate (20 μl in 500 μl MeCN). The mixture was stirred for 15 min at 80 °C. The product was purified by distillation at 130 °C. The product was analyzed using radio HPLC. HPLC conditions: Chromolith® SpeedROD RP-18 endcapped 50–4.6 HPLC column; solvent: 0–6 min: 10% MeCN: 90% H_2O; flow rate: 1.5 ml min^{-1}, 6–7 min: 80% MeCN: 20% H_2O; flow rate: 1.5 ml min^{-1}, 7–8 min: 10% MeCN: 90% H_2O; flow rate: 1.5 ml min^{-1}.

Radiolabeling of folic acid + 4-(azidoacetyl)catechol@Fe_3O_4 NPs with 5-[^{18}F]Fluoro-1-pent-4-ynyl. The synthesized compound 5-[^{18}F]Fluoro-1-pent-4-ynyl was used for the radiolabeling of the nanoparticles. Therefore, a copper-catalyzed Huisgen cycloaddition was carried out. Stock solutions of $CuSO_4$, L-histidine and NaAs were prepared to reduce the weighting error. 25 mg of $CuSO_4{\cdot}5\ H_2O$ (0.1 mmol), 39 mg of L-histidine (0.25 mmol) and 98 mg of sodium ascorbate (0.49 mmol) were dissolved in 500 μL of H_2O each. The purified 5-[^{18}F]Fluoro-1-pent-4-ynyl was mixed with 50 μl of $CuSO_4{\cdot}5\ H_2O$ solution, 50 μl of L-histidine solution and 50 μl of NaAs solution. 10 mg of folic acid + 4-(azidoacetyl) catechol@Fe_3O_4 nanoparticles were dispersed in 10 ml of dest. H_2O and added. The mixture was stirred for different times and different temperatures.

Direct radiolabeling of different nanoparticles. Aqueous [^{18}F]Fluorid was trapped on a SepPAK Light Water Accell™ Plus QMA cartridge (Waters GmBH, Eschborn, Germany), washed with methanol (1 ml), and eluted with tetraethylammonium bicarbonate solution (5 mg in 500 μl MeOH).

Methanol was evaporated under an argon stream at 40 °C and 500 mbar within 2–4 min. The nanoparticles (tosylate@γ-Fe_2O_3 nanospheres, folic acid + Tosylate@Fe_3O_4 nanoparticles or tosylate + dopamine@Fe_3O_4 nanoparticles) were dispersed in different solvents and directly mixed with the residue. The reaction time and temperature were varied.

Synthesis of [^{18}F]FET. [^{18}F]FET was produced at the cyclotron facility of INM-5 (Forschungszentrum, Jülich) as described previously.[52]

Cell culture. MCF7 breast tumor cells were obtained from DSMZ GmbH (Braunschweig, Germany). MCF-7 cells were cultured in EMEM supplemented with insulin (10 μg ml^{-1}), NAA (1%), FBS (10%) and penicillin/streptomycin (1%). The cells were cultured in 75 ml flasks containing 10 ml of the culture medium under a humidified atmosphere of 5% CO_2/95% air at 37 °C for 4–5 days until they reached 80–90% confluency. The cells were seeded into 12-well plates (10^5 cells per well containing 1 ml medium) for 24 h before the beginning of the cellular uptake experiments.

Cellular uptake experiments. [^{18}F]Dopamine@Fe_3O_4 nanoparticles, [^{18}F]folic acid@Fe_3O_4 nanoparticles and [^{18}F]FET (100–150 kBq per well; 1 ml) were added and the cells were incubated at 37 °C for 1 and 2 h. Thereafter, the cells were washed two times with medium (1 ml), trypsinized, harvested and the accumulated radioactivity was measured in a γ-counter (Wizard 1470, PerkinElmer, MA, USA). Each experiment was carried out in triplicate. The cellular uptake of [^{18}F]dopamine@Fe_3O_4 nanoparticles, [^{18}F]folic acid@Fe_3O_4 nanoparticles and [^{18}F]FET obtained in experiments performed in parallel was compared using 2-way ANOVA followed by Sidak's multiple comparison test ($p < 0.05$).

Conflicts of interest

There are no conflicts to declare.

Acknowledgements

The authors would like to acknowledge the financial support and infrastructure provided by the University of Cologne in the frame of the Excellence Strategy and for supporting the UoC-Forum "Transformative Nanocarriers for RNA Transport and Tracking".

References

1 L. M. Nieves, J. C. Hsu, K. C. Lau, A. D. A. Maidment and D. P. Cormode, *Nanoscale*, 2021, **13**, 163–174.
2 S. Ilyas, M. Ilyas, R. van der Hoorn and S. Mathur, *ACS Nano*, 2013, **7**, 9655–9663.
3 B. Klębowski, J. Depciuch, M. Parlińska-Wojtan and J. Baran, *Int. J. Mol. Sci.*, 2018, **19**, 4031.
4 M. D. Mauricio, S. Guerra-Ojeda, P. Marchio, S. L. Valles, M. Aldasoro, I. Escribano-Lopez, J. R. Herance, M. Rocha, J. M. Vila and V. M. Victor, *Oxid. Med. Cell. Longev.*, 2018, **2018**, 6231482.
5 A. Jurewicz, S. Ilyas, J. Uppal, I. Ivandic, S. Korsching and S. Mathur, *ACS Appl. Nano Mater.*, 2020, **3**, 1621–1629.
6 L. Labrador-Páez, E. C. Ximendes, P. Rodríguez-Sevilla, D. H. Ortgies, U. Rocha, C. Jacinto, E. Martín Rodríguez, P. Haro-González and D. Jaque, *Nanoscale*, 2018, **10**, 12935–12956.
7 A. M. Renner, S. Ilyas, K. Wennhold, A. Szymura, S. Roitsch, H. A. Schlößer and S. Mathur, *Langmuir*, 2020, **36**, 14819–14828.
8 M. B. Schütz, S. Ilyas, K. Lê, M. Valldor and S. Mathur, *ACS Appl. Nano Mater.*, 2020, **3**, 5936–5943.
9 R. Haldavnekar, K. Venkatakrishnan and B. Tan, *Nat. Commun.*, 2018, **9**, 3065.
10 B. Lin, J. Wu, Y. Wang, S. Sun, Y. Yuan, X. Tao and R. Lv, *Biomater. Sci.*, 2021, **9**, 1000–1007.
11 S. M. Siribbal, J. Schläfer, S. Ilyas, Z. Hu, K. Uvdal, M. Valldor and S. Mathur, *Cryst. Growth Des.*, 2018, **18**, 633–641.
12 D. P. Cormode, P. C. Naha and Z. A. Fayad, *Contrast Media Mol. Imaging*, 2014, **9**, 37–52.
13 A. Dash, B. Blasiak, B. Tomanek, A. Banerjee, S. Trudel, P. Latta and F. C. J. M. van Veggel, *ACS Appl. Nano Mater.*, 2021, **4**, 1235–1242.
14 J. Kim, P. Chhour, J. Hsu, H. I. Litt, V. A. Ferrari, R. Popovtzer and D. P. Cormode, *Bioconjugate Chem.*, 2017, **28**, 1581–1597.
15 A. L. Bernstein, A. Dhanantwari, M. Jurcova, R. Cheheltani, P. C. Naha, T. Ivanc, E. Shefer and D. P. Cormode, *Sci. Rep.*, 2016, **6**, 26177.
16 J. Wang, Y. Jia, Q. Wang, Z. Liang, G. Han, Z. Wang, J. Lee, M. Zhao, F. Li, R. Bai and D. Ling, *Adv. Mater.*, 2021, **33**, 2004917.
17 J. Jeevanandam, A. Barhoum, Y. S. Chan, A. Dufresne and M. K. Danquah, *Beilstein J. Nanotechnol.*, 2018, **9**, 1050–1074.
18 R. A. Revia and M. Zhang, *Mater. Today*, 2016, **19**, 157–168.
19 G. Jarockyte, E. Daugelaite, M. Stasys, U. Statkute, V. Poderys, T.-C. Tseng, S.-H. Hsu, V. Karabanovas and R. Rotomskis, *Int. J. Mol. Sci.*, 2016, **17**, 1193.
20 Q. Feng, Y. Liu, J. Huang, K. Chen, J. Huang and K. Xiao, *Sci. Rep.*, 2018, **8**, 2082.
21 M. A. Abakumov, A. S. Semkina, A. S. Skorikov, D. A. Vishnevskiy, A. V. Ivanova, E. Mironova, G. A. Davydova, A. G. Majouga and V. P. Chekhonin, *J. Biochem. Mol. Toxicol.*, 2018, **32**, e22225.
22 S. Berke, A.-L. Kampmann, M. Wuest, J. J. Bailey, B. Glowacki, F. Wuest, K. Jurkschat, R. Weberskirch and R. Schirrmacher, *Bioconjugate Chem.*, 2018, **29**, 89–95.
23 B. D. Zlatopolskiy, J. Zischler, D. Schäfer, E. A. Urusova, M. Guliyev, O. Bannykh, H. Endepols and B. Neumaier, *J. Med. Chem.*, 2018, **61**, 189–206.
24 L. Feni, M. A. Omrane, M. Fischer, B. D. Zlatopolskiy, B. Neumaier and I. Neundorf, *Pharmaceuticals*, 2017, **10**, 99.

25 E. J. Keliher, T. Reiner, G. M. Thurber, R. Upadhyay and R. Weissleder, *ChemistryOpen*, 2012, **1**, 177–183.
26 A. R. Jalilian and J. Osso Jr., *Iran. J. Nucl. Med.*, 2017, **25**, 1–10.
27 C. J. Anderson and R. Ferdani, *Cancer Biother. Radiopharm.*, 2009, **24**, 379–393.
28 A. Sasikumar, A. Joy, M. R. A. Pillai, R. Nanabala and B. Thomas, *Clin. Nucl. Med.*, 2017, **42**, e126–e127.
29 E. A. Aalbersberg, B. J. de Wit-van der Veen, M. W. J. Versleijen, L. J. Saveur, G. D. Valk, M. E. T. Tesselaar and M. P. M. Stokkel, *Eur. J. Nucl. Med. Mol. Imaging*, 2019, **46**, 696–703.
30 N. K. Devaraj, E. J. Keliher, G. M. Thurber, M. Nahrendorf and R. Weissleder, *Bioconjugate Chem.*, 2009, **20**, 397–401.
31 L.-L. Zhang, W.-C. Li, Z. Xu, N. Jiang, S.-M. Zang, L.-W. Xu, W.-B. Huang, F. Wang and H.-B. Sun, *Eur. J. Nucl. Med. Mol.*, 2021, **48**, 483–492.
32 R. J. Hicks, P. Jackson, G. Kong, R. E. Ware, M. S. Hofman, D. A. Pattison, T. Akhurst, E. Drummond, P. Roselt, J. Callahan, R. Price, C. Jeffery, E. Hong, W. Noonan, A. Herschtal, L. J. Hicks, M. Harris, A. Hedt, B. M. Paterson and P. Donnelly, *J. Nucl. Med.*, 2019, **60**, 777–785.
33 H. D. Zacho, R. F. Fonager, J. B. Nielsen, C. Haarmark, H. W. Hendel, M. B. Johansen, J. C. Mortensen and L. J. Petersen, *J. Nucl. Med.*, 2020, **61**, 344–349.
34 C. Bouter and Y. Bouter, *Front. Med.*, 2019, **6**, 71.
35 P. K. Garg, S. J. Lokitz, L. Truong, B. Putegnat, C. Reynolds, L. Rodriguez, R. Nazih, J. Nedrelow, M. de la Guardia, J. K. Uffman, S. Garg and P. S. Thornton, *PLoS One*, 2017, **12**, e0186340.
36 J. W. Kiser, J. R. Crowley, D. A. Wyatt and R. K. Lattanze, *Front. Med.*, 2018, **5**, 143.
37 G. Luurtsema, H. H. Boersma, M. Schepers, A. M. T. de Vries, B. Maas, R. Zijlma, E. F. J. de Vries and P. H. Elsinga, *EJNMMI Radiopharm. Chem.*, 2016, **1**, 7.
38 M. Pretze, C. Wängler and B. Wängler, *Biomed Res. Int.*, 2014, **2014**, 674063.
39 T. H. Ribeiro, R. S. Filho, A. C. G. Castro, E. Paulino and M. Mamede, *Rev. Assoc. Med. Bras.*, 2017, **63**, 109–111.
40 Z. Sun, K. Cheng, F. Wu, H. Liu, X. Ma, X. Su, Y. Liu, L. Xia and Z. Cheng, *Nanoscale*, 2016, **8**, 19644–19653.
41 M. Takeuchi, T. Nihashi, A. Gafter-Gvili, F. J. García-Gómez, E. Andres, D. Blockmans, M. Iwata and T. Terasawa, *Medicine*, 2018, **97**, e12909.
42 M.-T. Zhu, W.-Y. Feng, Y. Wang, B. Wang, M. Wang, H. Ouyang, Y.-L. Zhao and Z.-F. Chai, *Toxicol. Sci.*, 2009, **107**, 342–351.
43 R. Weissleder, D. D. Stark, B. L. Engelstad, B. R. Bacon, C. C. Compton, D. L. White, P. Jacobs and J. Lewis, *Am. J. Roentgenol.*, 1989, **152**, 167–173.
44 S. Ilyas, N. K. Ullah, M. Ilyas, K. Wennhold, M. Iqbal, H. A. Schlößer, M. S. Hussain and S. Mathur, *ACS Biomater. Sci. Eng.*, 2020, **6**, 6138–6147.
45 L. Wortmann, S. Ilyas, D. Niznansky, M. Valldor, K. Arroub, N. Berger, K. R. J. Holmes and S. Mathur, *ACS Appl. Mater. Interfaces*, 2014, **6**, 16631–16642.
46 A. Szymura, S. Ilyas, M. Horn, I. Neundorf and S. Mathur, *J. Mol. Liq.*, 2020, **317**, 114002.
47 K. V. Korpany, D. D. Majewski, C. T. Chiu, S. N. Cross and A. S. Blum, *Langmuir*, 2017, **33**, 3000–3013.
48 M. Pretze, D. Pietzsch and C. Mamat, *Molecules*, 2013, **18**, 8618–8665.
49 J. P. Marshalek, P. S. Sheeran, P. Ingram, P. A. Dayton, R. S. Witte and T. O. Matsunaga, *J. Controlled Release*, 2016, **243**, 69–77.
50 P. Patra, S. Mitra, N. Debnath, P. Pramanik and A. Goswami, *Bull. Mater. Sci.*, 2014, **37**, 199–206.
51 A. M. Klester and C. Ganter, *Helv. Chim. Acta*, 1983, **66**, 1200–1209.
52 K. Hamacher and H. H. Coenen, *Appl. Radiat. Isot.*, 2002, **57**, 853–856.